Shaking table tests on a 5-storey unreinforced masonry structure strengthened by ultra-high ductile cementitious composites

Chen, Xi; Zhang, Yongqun ; Wang, Zhuolin ; Yu, Jiangtao ; Skalomenos, Konstantinos; Xu, Qingfeng

DOI:
10.1016/j.jobe.2022.104635

Shaking table tests on a 5-storey unreinforced masonry structure strengthened by ultra-high ductile cementitious composites

Xi Chen[a], Yongqun Zhang[a], Zhuolin Wang[a*], Jiangtao Yu[b], Konstantinos Skalomenos[c], Qingfeng Xu[a]

a. Shanghai Key Laboratory of Engineering Structure Safety, Shanghai Research Institute of Building Sciences (Group) Co., Ltd., Shanghai, PR China

b. Department of Disaster Mitigation for Structures of Structural, Tongji University, Shanghai, PR China

c. Department of Civil Engineering, The University of Birmingham, B15 2TT, Edgbaston, Birmingham, United Kingdom.

Abstract: Multi-storey unreinforced masonry structures have been widely used as residential building structures in China during the decade of 1970-1980. Recent earthquake events have shown that these buildings may exhibit severe damages due to their relatively brittle seismic resistance mechanism. The use of ultra-high ductile cementitious composites (UHDCC) layers can be an attractive minimal-disturbance strengthening option for masonry structures resulting in low intervention costs and quick construction. UHDCC is a high-performance engineered cementitious composite that offers a tensile strain capacity higher than 5%, thus significantly improving the low tensile strength and ductility of the masonry wall. To investigate the seismic behavior of UHDCC-strengthened masonry structures, shaking table tests were carried out on two three-dimensional 5-storey masonry structures including a conventional test structure (CS) and a strengthened test structure (SS). The results show that the proposed strengthening method can effectively improve the seismic performance of multi-storey unreinforced masonry structures due to the excellent cohesion achieved between the existing masonry walls and the UHDCC external strengthening layers. The strengthened method changes the damage state of masonry structures from shear failure to a more ductile failure, and the strengthened masonry walls can exhibit a multi-cracking response. The initial natural period of the SS specimen was found 0.58 times that of the CS specimen. The base shear and maximum roof drift of the SS specimen are 4.8 and 3.4 times that of the CS model, respectively. This study provides reference results for the application of UHDCC layers to strengthen multi-storey unreinforced masonry structures.

Keyword: unreinforced masonry structure; ultra-high ductile cementitious composites; shaking table testing; seismic strengthening; multi-cracking

1. Introduction

Multi-storey unreinforced masonry structures were widely used as residential building structures in China during the decade 1970-1980. According to statistics, currently there are about 50,000 residential masonry buildings only in Shanghai City that cover an area of 130 million m^2. Because of several economical and historical reasons, masonry structures in China appear to have the following weaknesses: a) most of them have not been designed adequately against earthquakes, for instance reinforced concrete (RC) tie column or RC tie beams have not been considered in the original design, while some of the structures were designed ignoring seismic loads completely; b) the material strength of the structural system is generally very low. The strength of masonry mortar may not be higher than 2.5MPa; c) large openings have been constructed in the walls of the longitudinal direction of the buildings for daylighting purposes while precast RC panels with no effective anchorage were used as floors. Both of these construction practices lead in a poor structural integrity and lateral resistance. Because of the above reasons, earthquake events [1-4] have shown that multi-storey unreinforced masonry structures may suffer severe damages, including collapse, resulting in huge economic losses and casualties. The large number of such structures, particularly in the downtown area of Shanghai, makes their demolition or deconstruction very expensive and authorities often prefer to bring the existing structures stock to higher safety standards through low-cost, quick and minimal-disturbance strengthening solutions.

Various seismic strengthening technologies have been investigated and developed to improve the seismic performance of masonry structures so far. Surface treatment, including ferrocement, reinforced plaster and shotcrete [5][6][7], are widely used. The effectiveness of these methods has been validated. Although these strengthened methods are low-cost solutions and can be applied by unskilled labor, they require bonding a new material layer with thickness of more than 60 mm to the existing masonry walls. Such layers may increase structural weight significantly and reduce living space, while they take a quite long time to construct them [8][9]. External bonded fiber reinforced polymer (FRP) strips or laminates [10][11] is an alternative conventional method to strengthen masonry structures. FRP materials are light and can effectively improve the in-plane and out-of-plane lateral capacity of masonry structures while they are relatively easy to implement them in practice. However, FRP materials exhibit some disadvantages, such as poor ductility, and weak anchorage or bonding, which may cause brittle behavior and debonding defects.

In recent years, engineered cementitious composites (ECC) have been developed which can be obtained through a reasonable design of the matrix, fiber, and interface properties of the cementitious composites [12], and are characterized by multi-cracking behaviour and high strain-hardening performance [13][14]. Compared to the traditional strengthening materials (e.g. concrete, steel strip, FRP), ECC have lower elastic modulus and higher ductility under tension and shear, while their ultimate tensile strain can reach 0.5% ~ 3.0%. Based on the above advantageous mechanical properties, ECC were developed as an externally bonded material for strengthening masonry walls. The investigations showed that the ECC strengthening method can significantly improve the in-plane stiffness, lateral capacity, and ductility of masonry walls [15-17]. Moreover, the use of ECC to improve the out-of-plane behavior and load-carrying capacity of masonry walls has also been confirmed [18][19]. Deng et al. [20][21] developed a new type of ECC material, named high-ductility concrete (HDC), to strengthen masonry walls. The new composite material has been validated in a two-storey masonry structure through quasi-static and shaking table tests which demonstrated that the strengthened masonry structure may exhibit a better seismic performance. However, the strengthened low-rise masonry structure shows slight rocking behavior, which will be more significant in multi-storey masonry structures, which may lead to overall overturning failure of multi-storey masonry structures. Therefore, the effectiveness of using ECC to strengthen multi-storey unreinforced masonry structures remains to be investigated.

Yu et al. [22][24] developed a new-type of ECC that offers a superior tensile strain capacity (i.e., more than 5%), called ultra-high ductile cementitious composites (UHDCC). Experimental and analysis results showed that UHDCC can effectively strengthen reinforced concrete structures [25][26]. The application of UHDCC to strengthen multi-storey unreinforced masonry structures is yet to be investigated. The present study investigates the effectiveness of using UHDCC layers and ECC layers to improve the seismic performance of multi-storey unreinforced masonry structures.

Two three-dimensional 5-storey masonry structures were firstly designed according to the construction regulations and code of practice of Shanghai in 1970s. One test structure was strengthened by UHDCC and ECC, while the other one was used as a reference structure (conventional structure). Shaking-table tests were conducted to impose various intensity levels of seismic excitations to the test structures. Their dynamic characteristics and seismic behavior were analyzed and compared in detail for understanding the effectiveness of the proposed strengthening method.

2. Experimental program

2.1 Details of the test models

2.2.1 Conventional structure

Shaking table tests of a conventional test structure (CS) and a corresponding strengthened test structure (SS) were conducted. The CS model, as shown in Fig. 1, is one quarter scale model of a typical 5-storey masonry residential building designed in 1970s in the Southern China. The width of the structure in the longitudinal (X-direction) and lateral (Y-direction) direction is 2,100 mm and 2,325 mm, respectively. Each storey has 750 mm height and the entire masonry structure is mounted on a 300 mm thick foundation beam. Reinforced concrete (RC) tie columns are not constructed. The thickness of masonry walls is scaled down to 60 mm using bricks of dimensions (length × width × height) of 115 mm × 60 mm × 53 mm. A mortar joint of 5 mm thickness is employed.

RC tie beams are constructed under the floor slabs of the 2nd, 4th and 5th storey, respectively, while the cross-section of the RC tie beam is 60 mm × 45 mm (Fig. 2a). The RC tie beams are prepared using micro-concrete and have four longitudinal reinforcing bars of 3.5 mm diameter and steel ties of 2.2 mm diameter spaced horizontally every 50 mm. Lintels are constructed on the top of the door and window openings having a cross-section of 60 mm × 75 mm (Fig. 2b). Lintels are poured with micro-concrete and had five longitudinal reinforcing bars of 3.5 mm diameter and steel ties of 2.2 mm diameter spaced horizontally every 25 mm.

Precast RC panels are constructed to serve as floor slabs, i.e., YKB-1 and YKB-2 in Figs. 2c and 2d, having dimensions of 300 mm × 900 mm and 300 mm × 600 mm, respectively. According to the similarity equations, all precast RC floor panels should be 25 mm thick. However, considering construction issues and the fact that precast slabs with 25 mm thickness cannot support safely the mass induced by blocks sit on them, the thickness of the precast floor slab in the test specimen is increased to 30 mm. The extra mass caused by the thicker floor slab is deducted from the mass blocks.

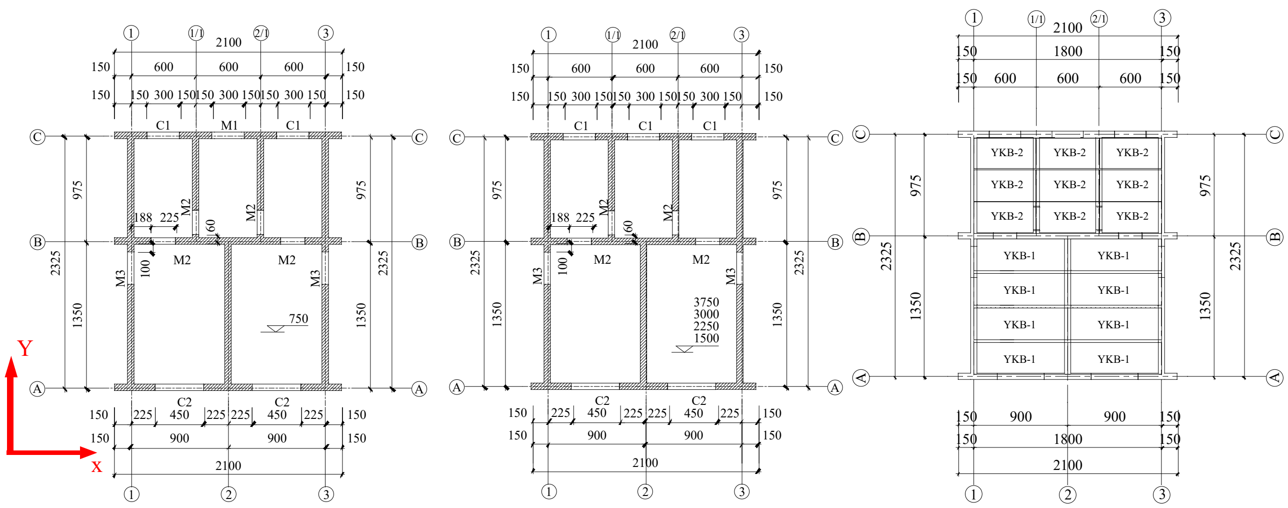

(a) 1st storey (b) 2nd to 5th storey (c) The layout of precast RC floor panels

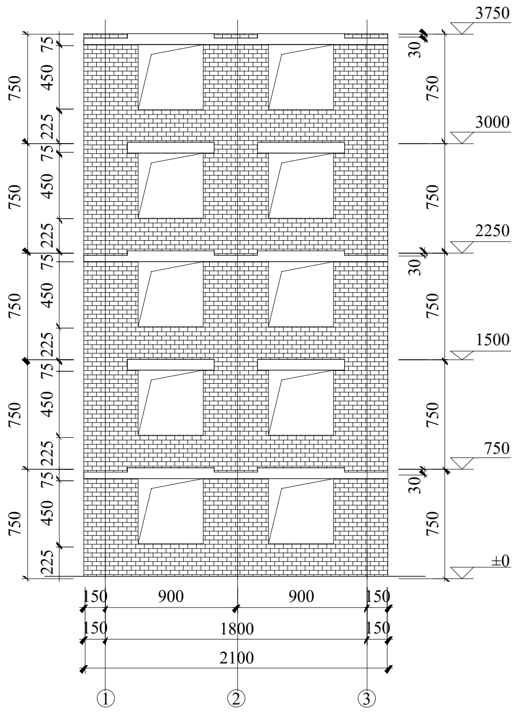

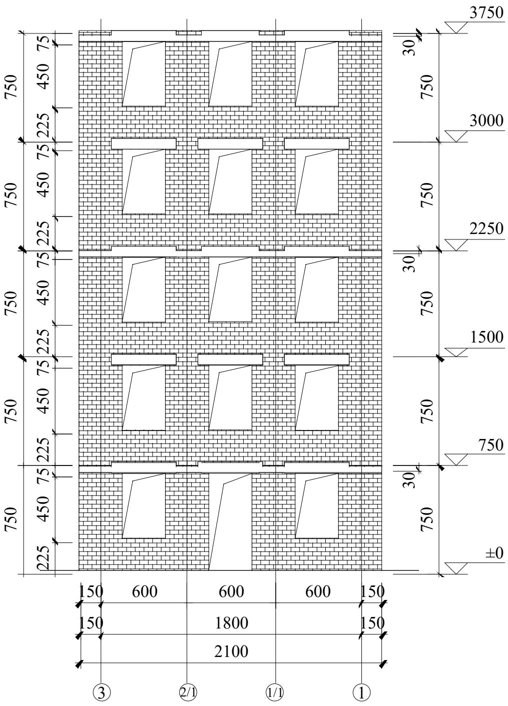

(d) South elevation (e) North elevation

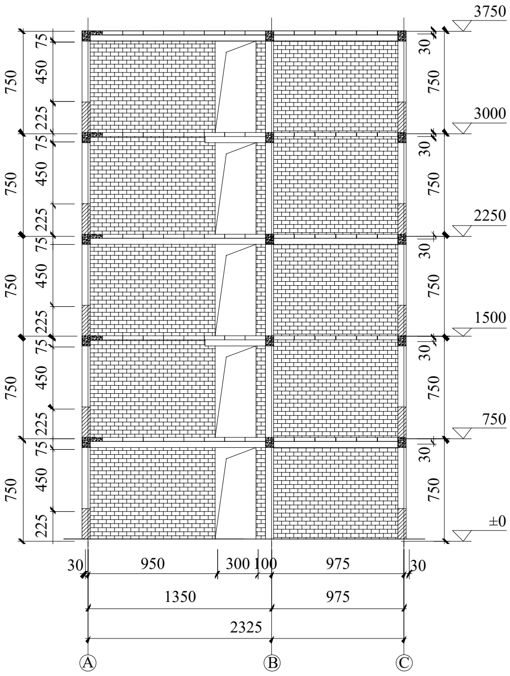

(f) West elevation (g) Overview of CS

Fig. 1. Dimension and plane layout of CS test (mm).

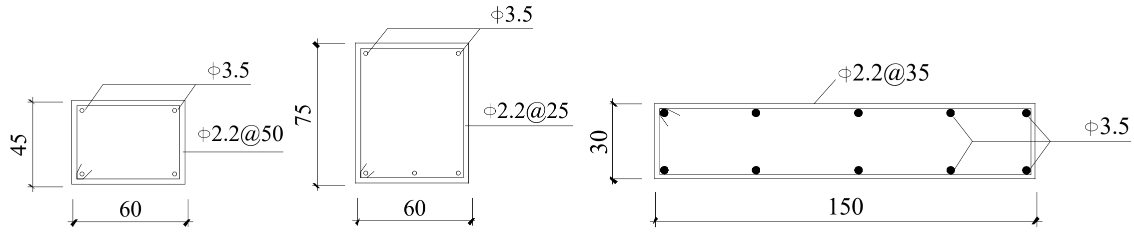

(a) RC tie beam (b) Lintel (c) YKB-2

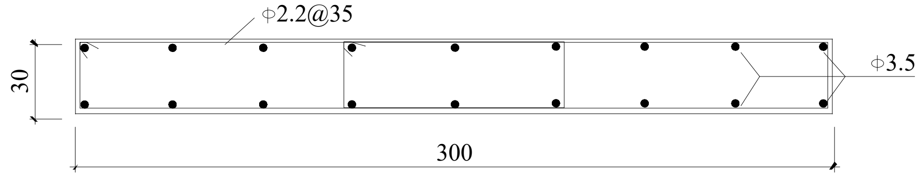

(d) YKB-1

Fig. 2. Cross-section of (a) RC tie beam, (b) lintel, and (c) precast RC floor panels (in mm).

2.2.2 Strengthened structure

To evaluate the effectiveness of various strengthening methods, the masonry structure was strengthened by either engineered cementitious composite (ECC) layers or ultra-high ductile cementitious composite (UHDCC) layers. Firstly, the masonry structure strengthened by single-sided engineered cementitious composite (ECC) layers was tested by shaking table tests, the ECC layers (10 mm) were cast onto the outside surface of the masonry walls at grid line “A” and “C” to enhance structural integrity. The results showed that the failure mode of the strengthened structure is rocking failure, which is manifested by the overall rocking of the superstructure (2nd - 5th storey of the structure). The main cracks were the horizontal cracks penetrating all masonry walls at the top of the 1st storey, and the diagonal cracks at the corner of the wall openings in the 1st and 2nd storey of the structure were observed. Besides, shear failure occurred in the masonry wall at grid line “B” in the 1st storey, the cracks extended from four corners to the center of masonry wall and intersected to form an “X” shaped crack.

Subsequently, the ECC layers of the bottom two storeys were removed, and UHDCC layers were employed to strengthen the damaged structure for conducting a second test. The experimental results of the second test are provided in this study.

The steps of the strengthened method followed in this study are as follows:

(1) Since damage mainly occurred in the 1^{st} and 2^{nd} storey of the structure during the first test, the ECC layers of these storeys were removed. Over the stripped walls, masonry cracks were measured and those greater than 0.5 mm wide were filled with epoxy mortar, while smaller cracks were not treated. A masonry wall which heavily damaged in the 1^{st} storey was rebuilt. The detailed configuration of the strengthening method is shown in Fig. 3.

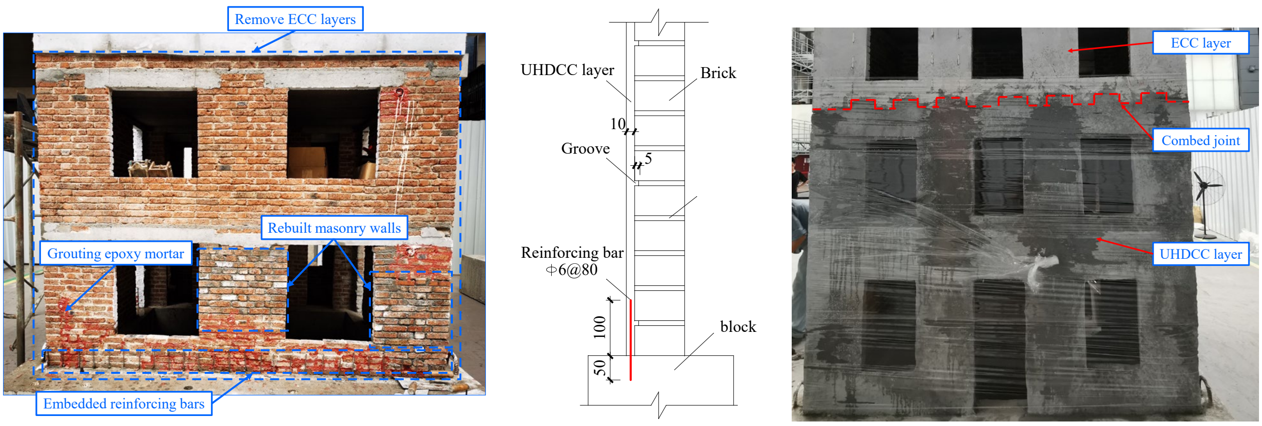

(a) Existing damage repaired (b) Detailed configuration of the connection (c) UHDCC layer setting

Fig. 3. Detailed configuration of the strengthening method.

(2) The UHDCC-strengthened scheme was carried out in this phase. The dimension and layout of the UHDCC layers are shown in Fig. 4. To achieve a minimal-disturbance during construction, the

external masonry walls were strengthened using UHDCC layers with a thickness of 10 mm. UHDCC layers were applied at masonry walls located in the grid line “A” and “C” of the 1st and 2nd storey, as shown in Fig. 4. A combed joint was considered to ensure that both the UHDCC layers and ECC layers work together, as shown in Fig. 3c, thus avoiding any damage concentration in the interface of the two materials. Moreover, UHDCC layers were applied at the masonry walls located in the grid line “1” and “3” of the 1st, 2nd, and 3rd storey, as shown in Fig. 4. Considering the low shear demand on the 4th and 5th storey of the structure, UHDCC strips with a width of 110 mm were used to strengthen the masonry walls located in the grid line “1” and “3” of the 4th and 5th storey of the structure, as shown in Fig. 4e.

To ensure that the existing masonry walls and the UHDCC layers work together, horizontal grooves with a depth of 5 mm are arranged in horizontal mortar layers every 240mm vertically, as shown in Fig.3. The effect of the groove is to increase the surface roughness of masonry walls, and the UHDCC layers are embedded into the grooves to enhance the bonding performance between the masonry walls and the UHDCC layer.

To prevent slippage between the UHDCC layers and the foundation block, the top surface of the foundation block was roughened. Then, reinforcing bars were embedded every 80 mm pitch distance along the horizontal direction. Reinforcing bars of 6 mm diameter were emended for a length of 50 mm into the foundation block and for a length of 100mm into the UHDCC layers (Fig. 3).

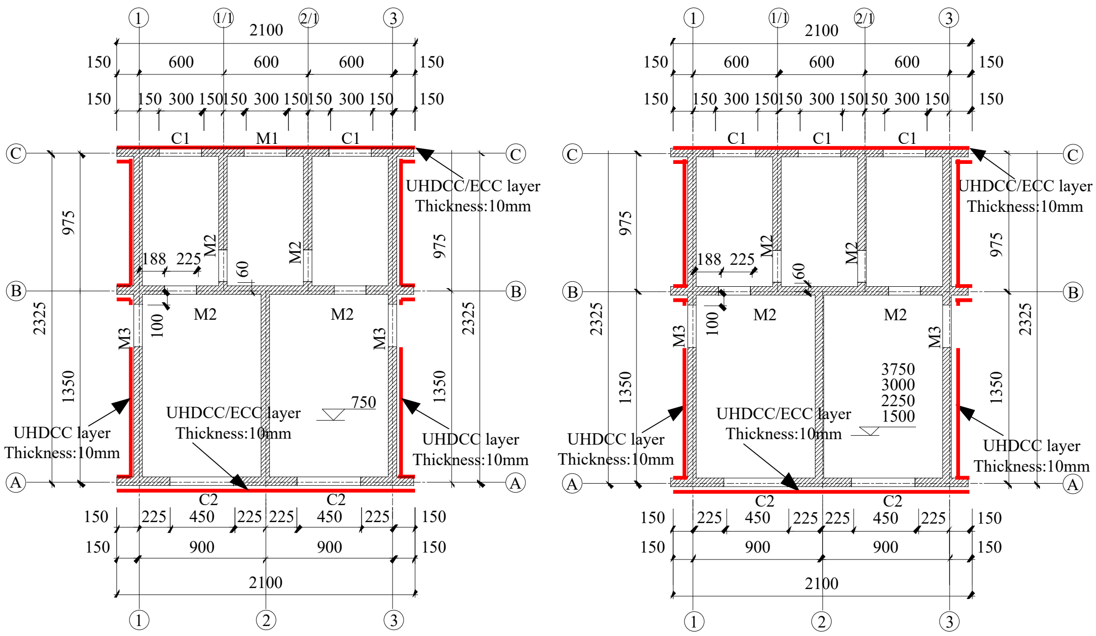

(a) 1st storey (b) 2nd to 5th storey

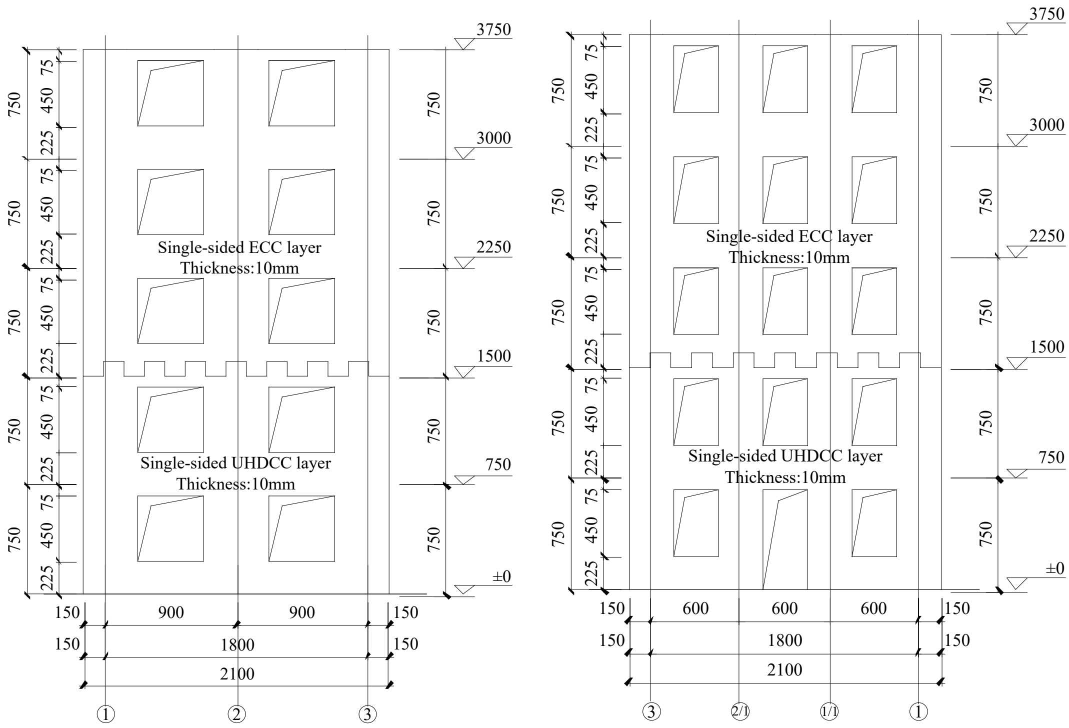

(c) South elevation (d) North elevation

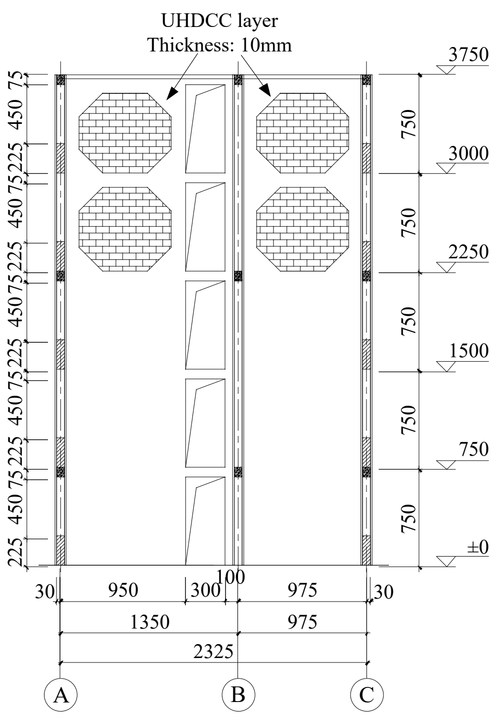

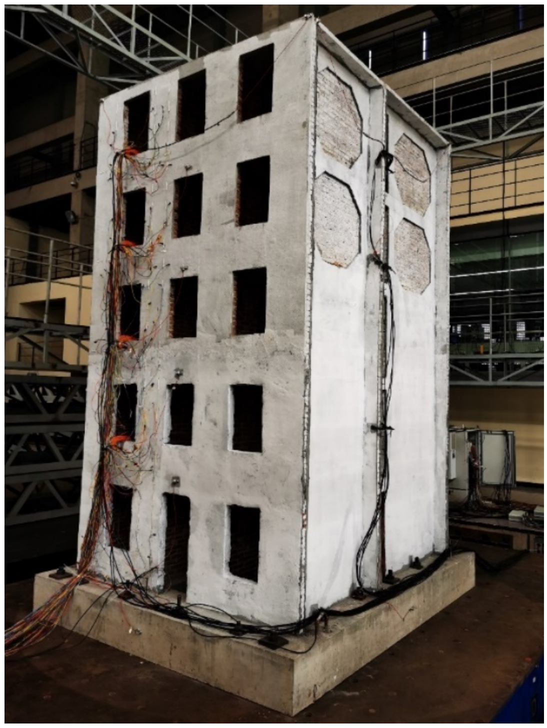

(e) West elevation (f) Overview of SS

Fig. 4. Dimension and plane layout of SS test (mm).

2.2 Material properties

To investigate the actual seismic performance of the masonry structure, structural materials used in multi-storey masonry residential buildings in the Southern China were selected, such as, clay brick and mixed mortar for masonry walls. As stipulated in Chinese code JGJ/T 70-2009 [28], the compressive strength of mortar was tested on 70.7 mm cubes, and the bed-joint sliding strength of the masonry $f_{v,0}$ was determined by direct shear tests on three bricks bonded together with two mortar layers without transverse restraint. The masonry compressive strength f_m was tested according to the Chinese code GB/T 50129–2011 [29]. The measured average compressive strength of a brick and mortar for the CS specimen were 14.7 MPa and 1.5 MPa, respectively, and those of the SS specimen were 17.8 MPa and 1.3 MPa, respectively. The measured compressive strength and bed-joint sliding strength of the masonry wall for the CS specimen were 3.3 MPa and 0.2 MPa, respectively, and those of the SS specimen were 3.5 MPa and 0.2 MPa, respectively.

The compressive strength and tensile strength of the micro-concrete used for the lintels of the CS specimen were 19.8 MPa and 1.7 MPa, respectively, and those of the SS specimen were 23.6 MPa and 1.9 MPa. The yield tensile strength of the 2.2-mm-reinforcing steel bars of the CS specimen and the SS specimen was 451.2 MPa and 420.9 MPa, respectively. The yield tensile strength of the 3.5-mm-reinforcing steel bars of the CS and SS specimens was 412.9 MPa and 405.7 MPa, respectively.

The ECC is composed of Portland cement, fly ash, sand, water proportions of 1:2.33:0.72:0.96, and polyvinyl alcohol (PVA) fibres with a 2% volume content. The compressive strength of ECC was obtained from test on 50 mm cubes, while the tensile strength of ECC was obtained from test on dogbone-shaped specimens (height 100 mm, width 30 mm, thickness 12 mm). The measured compressive strength and tensile strength of ECC were 36.0 MPa and 4.5 MPa, respectively, and the average ultimate tensile strain reached 2.8%.

The UHDCC is composed of Portland cement, fly ash, sand, water proportions of 1:1.20:0.80:0.55. High-range water-reducer (also named super plasticizer) admixture content was 4.8 g/L and polyethylene (PE) fibres with a 0.8% volume content [23]. The material tests of UHDCC were the same as those of ECC. The measured compressive strength and tensile strength of UHDCC were 36.9 MPa and 3.9 MPa, respectively, and the average ultimate tensile strain reached 6.1%.

2.3 Similitude design

The model structures were designed according to the dimension and capacity of the shaking table, and the similitude scaling factors between the prototype structure and the model structures were determined considering consistent material properties, as shown in Table 1.

The mass of the model specimens is determined from the weight of the structural members and the following additional components: (a) a roof dead load of 4.0 kN/m^2, and a roof live load of 0.5 kN/m^2; (b) a floor dead load 3.5 kN/m^2, and a roof live load of 2.0 kN/m^2. The resulting mass of the CS specimen was 6.7 t. An additional mass of 2.2 t was employed by considering the prescribed similitude scaling factors for mass. The foundation block used for testing had a mass of 3.4 t, making the total mass of the CS specimen approximately 12.3 t. The masses of the superstructure, foundation, and total mass of the SS specimen were 9.4 t, 3.4 t and 12.8 t, respectively.

Table 1 Similitude scaling factors.

Parameter	Relationship	Dimension	Scaling factor
Length (l)	S_l	L	1/4
Strain	$S_\varepsilon = S_\sigma/S_E$	-	1
Modulus of elasticity (E)	S_E	FL^{-2}	1
Density (ρ)	$S_\rho = S_E/(S_l S_a)$	FT^2L^{-4}	8/5
Mass (m)	$S_m = S_\rho S_l^3$	FT^2L^{-1}	1/40
Stress (σ)	$S_\sigma = S_E$	FL^{-2}	1
Time (t)	$S_t = S_l\,(S_E/S_\rho)^{-0.5}$	T	1/3.162
Frequency (ω)	$S_\omega = S_l^{-1}(S_E/S_\rho)^{0.5}$	T^{-1}	3.162
Acceleration (a)	$S_a = S_E/(S_l S_\rho)$	LT^{-2}	2.5

2.4 Instrumentation

Twelve acceleration sensors and fourteen displacement sensors were installed on the masonry structures to obtain the global dynamic responses. The layout of the sensors of the structure models are shown in Fig. 5. The acceleration sensors, named A*x** and A*y**, were utilized to collect the horizontal acceleration response in X- and Y-direction, respectively. Similarly, the displacement sensors, named D*x** and D*y**, were utilized to collect the horizontal displacement response in X- and Y-direction, respectively. The * represents the sensor number.

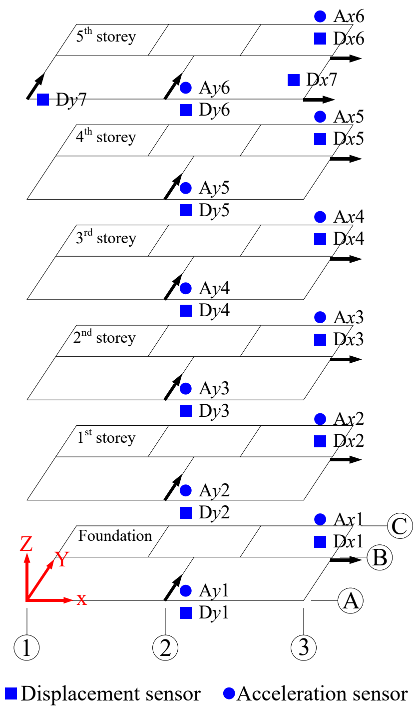

Fig. 5. Arrangement of sensors.

2.5 Test procedure

The main purpose of the shake table tests was to assess the seismic response of the masonry structure strengthened by UHDCC layers at different levels of seismic intensity and different site categories. Three different seismic ground motions were selected as input excitations: the 1940 El Centro and the 1952 Taft ground motions, and an artificially generated ground motion suitable for Shanghai City (SHW2), the seismic ground motions with real period are illustrated in Fig. 6. The El Centro, Taft, and Shanghai ground motions were applied in sequence under each seismic intensity level. Seven intensity levels of each seismic motion were generated, as shown in Table 2. According to the Chinese *code for seismic design of buildings* [30] and the acceleration similitude factor (S_a = 2.5), the target peak ground accelerations (PGA) for a frequent, design-basis, and major event was considered 0.0875g, 0.250g, and 0.550g, respectively. Therefore, three phase tests (PGAs of 0.0875g, 0.250g, and 0.550g) were carried out for the CS specimen, and an additional four testing phases (PGAs of 0.775g, 1.000g, 1.275g, and 1.550g) were carried out for the SS specimen due to its greater deformability, as described in Table 2. Considering the poor seismic performance of masonry structures, only X-direction seismic excitations were carried out for the CS test. Before and after each series of the six excitations at a given intensity level, white noise scanning (PGA = 0.050 g) was performed in both horizontal directions to obtain the dynamic characteristics of the two models. The CS specimen suffered serious damage under seismic motions of a PGA equal to 0.550g, thus the white noise scanning was performed only after imposing the Shanghai ground motion with PGA = 0.550g (see Table 2 – Test No. 20), and then the test was stopped. The SS specimen suffered serious damage under the Taft ground motion for a PGA equal to 1.550g, so the white noise scanning was performed after imposing the Taft ground motion in X-direction with PGA = 1.550g (see Table 2 - Test No. 46), and then the test was stopped.

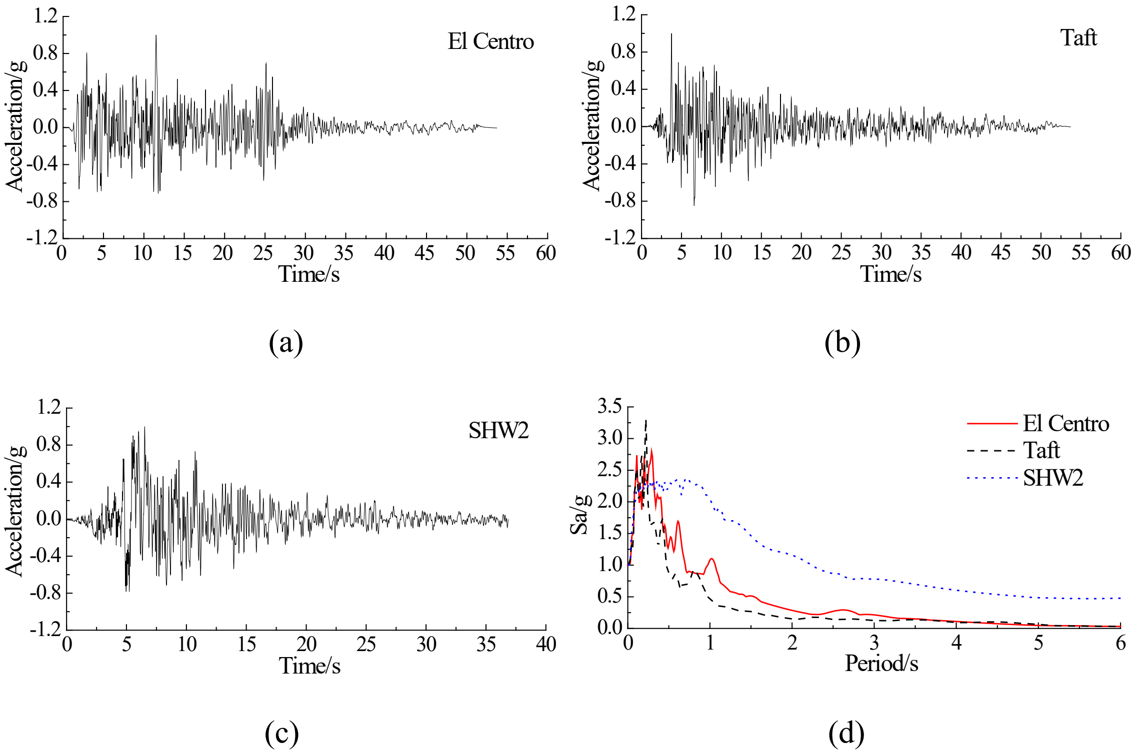

Fig. 6. Acceleration time histories and spectra for the selected seismic motions

Table 2 Test conditions and loading sequence (PGA/g).

Test No.	Input motion	PGA/g
1	White noise 1	0.050
2-7	El Centro-X, El Centro-Y, Taft-X, Taft-Y, SHW2-X, SHW2-Y	0.0875
8	White noise 2	0.050
9-14	El Centro-X, El Centro-Y, Taft-X, Taft-Y, SHW2-X, SHW2-Y	0.250
15	White noise 3	0.050
16-21	El Centro-X, El Centro-Y, Taft-X, Taft-Y, SHW2-X, SHW2-Y	0.550
22	White noise 4	0.050
23-28	El Centro-X, El Centro-Y, Taft-X, Taft-Y, SHW2-X, SHW2-Y	0.775
29	White noise 5	0.050
30-35	El Centro-X, El Centro-Y, Taft-X, Taft-Y, SHW2-X, SHW2-Y	1.000
36	White noise 6	0.050
37-42	El Centro-X, El Centro-Y, Taft-X, Taft-Y, SHW2-X, SHW2-Y	1.275
43	White noise 7	0.050
44-49	El Centro-X, El Centro-Y, Taft-X, Taft-Y, SHW2-X, SHW2-Y	1.550

50	White noise 8	0.050

* Shaded entries indicate tests of the CS specimen; "*-X" and "*-Y" represents the direction of the input motion.

3. Experimental results

3.1 Behaviour and failures

3.1.1 CS test specimen

During initial PGA = 0.0875g test stages, thin horizontal cracks appeared in the bed-joints at the bottom of the masonry walls in the X-direction. By PGA = 0.250g, two diagonal stepped cracks with a width of 0.1mm were observed in the wall between the two openings at grid line "A" of the 1st storey (Fig. 7a). After imposing the El Centro ground motion with PGA = 0.550g, several diagonal stepped cracks and horizontal bed-joint cracks were observed at the corners of the wall openings in the X-direction of the 2nd and 3rd storey (Figs. 7b and 7c), the maximum width of diagonal stepped cracks reached 0.5mm. After PGA = 0.550g test stages, the cracks at the corners of the wall openings of the 3rd storey continued to develop and connected with the cracks of the 2nd storey, thus forming vertical cracks through the masonry wall (Fig. 7d). The diagonal stepped cracks propagated to form X-shaped cracks at the internal wall of the 2nd storey, which caused serious shear failure and local collapse (Figs. 7e and 7f). Due to the collapse of the internal wall, the test sequence for the CS specimen was terminated after PGA = 0.550g test stages.

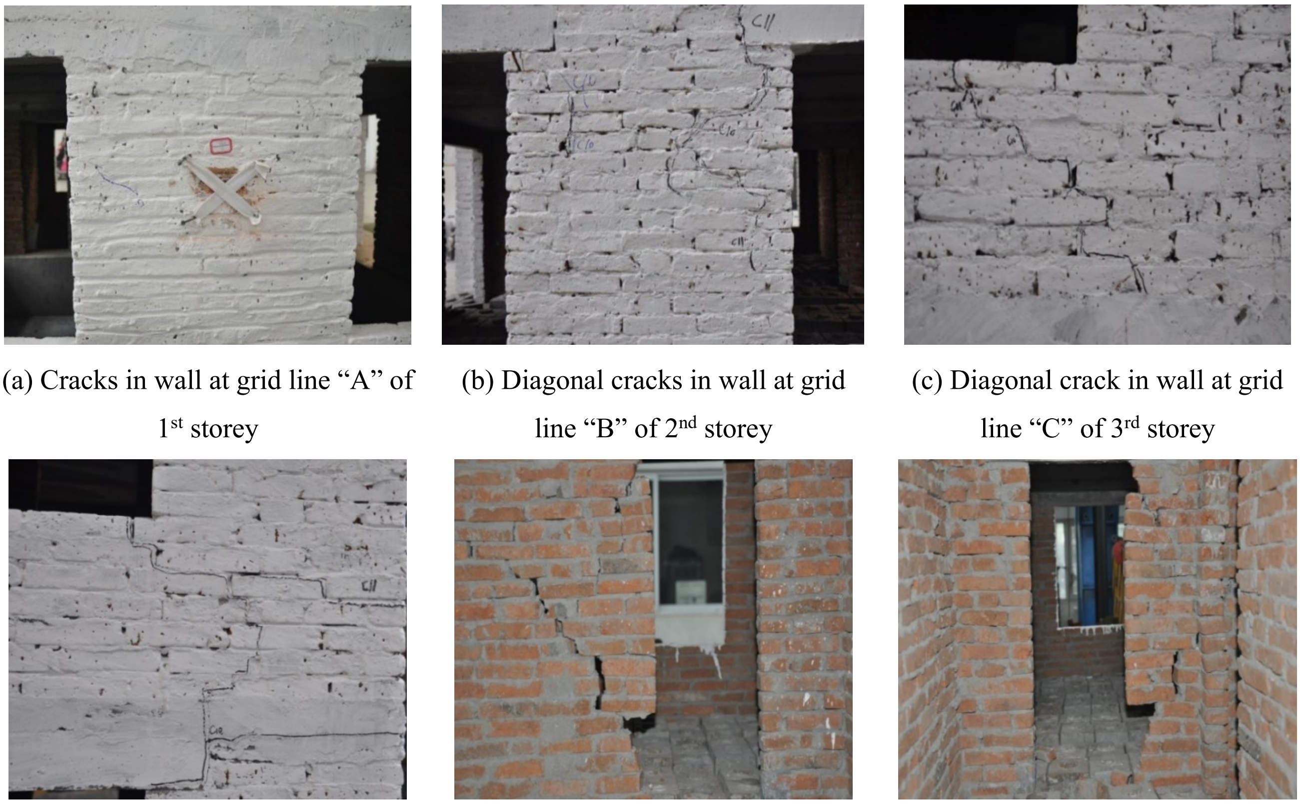

(a) Cracks in wall at grid line “A” of 1st storey

(b) Diagonal cracks in wall at grid line “B” of 2nd storey

(c) Diagonal crack in wall at grid line “C” of 3rd storey

(d) Vertical cracks in wall at grid line “C” of 3rd storey

(e) Shear failure in wall at grid line “B” of 2nd storey

(f) Collapse of masonry wall at grid line “B” of 2nd storey

Fig. 7. Observed damages in CS specimen testing.

3.1.2 SS test specimen

There was not visible damage during initial PGA = 0.0875g test stages for the SS specimen. During PGA = 0.250g test stages, many horizontal cracks, which appeared as multi-cracking, were observed in the left wall beside the openings at grid line “A” and “C” of 1st storey (Figs. 8a and 8b). Besides, several cracks appeared at the corners of the wall openings in the 1st storey. With the increasing of seismic intensity, new cracks appeared at the corners of the wall openings of 2nd and 3rd storey, and the existing cracks continued to develop, and the X-shaped cracks were formed in the internal wall at grid line “B” of 1st and 2nd storey. By PGA = 1.000g, new cracks appeared next to the existing cracks at the corners of the wall openings, forming a multi-cracking pattern, and continuously developed to run through the wall between openings at grid line “A” and “C”. During PGA = 1.275g test stages, the cracks at the corners of the wall openings at grid line “C” of the 2^{nd} storey continued to develop and connected with the cracks of 1^{st} storey to form vertical cracks (Fig. 8c). Horizontal cracks appeared at the left end of the junction of ECC layer and UHDCC layer. Horizontal cracks were observed at the bottom of grid line “1” of 3^{rd} storey and grid line “3” of 2^{nd} storey.

By PGA = 1.550g, bending failure occurred at the 3^{rd} storey, the bending cracking of the wall was quite large with a maximum width of 3.2mm, while the upper part of the wall had an out-of-plane displacement of 4.3mm (Figs. 8d and 8e). Although there are cracks at the junction of ECC layer and UHDCC layer, there is no relative sliding, indicating that the layers can still work together. The middle masonry walls between openings showed rocking failure (Fig. 8f). The shear cracks of the wall between the openings of the 1^{st} and 2^{nd} storey continued to extend, resulting in a multi-cracking behavior (Fig. 8g). The bricks at the upper corner of the wall at grid line “B” of 1^{st} storey fell off (Fig. 8h), and the masonry wall at grid line “B” of 3^{rd} storey locally collapsed (Fig. 8i).

Due to the serious bending failure of the 3^{rd} storey, and the local collapse of the internal wall, the structure lost its lateral capacity. The test sequence was ended after imposing the Taft ground motion in X-direction. During the test, the UHDCC layers were well connected with the masonry walls and they could work together efficiently.

(a) Horizontal cracks in wall at grid line "C" of 1st storey
(b) Horizontal cracks in wall at grid line "A" of 1st storey
(c) Shear cracks in wall at grid line "C" of 2nd storey
(d) Cracks in wall at grid line "A" of 3rd storey
(e) Cracks in masonry wall at grid line "C" of 3rd storey
(f) Horizontal cracks in short wall limb at grid line "C" of 3rd storey
(g) Shear cracks in wall at grid line "A" of 2nd storey
(h) Shear failure in wall at grid line "B" of 1st storey
(i) Collapse of masonry wall at grid line "B" of 3rd storey

Fig. 8. Observed damage during SS specimen testing.

3.2 Dynamic properties

The level of structural damage and stiffness deterioration can be quantitatively estimated by analyzing the dynamic properties. White noise excitations with a PGA of 0.050g were employed between the increasing levels of seismic intensity to study the changes of the dynamic properties alongside with the damage growth. The fundamental frequencies of the CS specimen and SS specimen, analyzed by frequency response functions, are shown in Table 3. The ratios given in Table

3 are the calculated frequency f over the initial frequency f_0.

The initial frequency of the CS specimen was 7.94Hz in the X-direction, while initial frequencies of SS specimen were 13.70Hz and 18.87Hz in the X- and Y-directions, respectively. The initial frequency of the SS specimen was found 1.73 times that of the CS specimen, the reason is that the elastic stiffness of the masonry structure is significantly improved, and the seismic load applied to the structure also increases, resulting in increasing dynamic amplification. The frequency of the SS specimen in X-direction was found to be larger than that in Y-direction because of the presence of relatively large openings in the walls in X-direction.

As the input PGA increased, the structural damage accumulated and the stiffness deteriorated, thus resulting in associated reductions of the fundamental frequency. Based on the identification of the dynamic properties of the structure after PGA = 0.550g test stages, the f/f_0 ratio of the CS specimen in X-direction decreased to 0.382 from 1.0, while the corresponding ratios for the SS specimen in X- and Y-direction decreased only to 0.820 and 0.883, respectively. Moreover, the CS specimen lost its lateral capacity after PGA = 0.550g test stages, and its failure mode is fully brittle. For the same acceleration input, only a slight damage was identified in the SS specimen. After PGA = 1.550g test stages, the f/f_0 ratio in SS specimen in X- and Y-direction decreased to 0.255 and 0.505, respectively. Compared to SS specimen, stiffness deterioration was found to be significant in the CS specimen as the seismic intensity increased. It was proved that the proposed strengthening method shall effectively improve the seismic performance of unreinforced masonry structures under a wide range of seismic intensities, thus preventing masonry structures from heavy damages or sudden collapse against design-basis and major earthquakes or earthquake sequential events [31].

Table 3 Variation of frequencies and natural periods of CS and SS specimens.

White noise	CS specimen		SS specimen			
	X-direction		X-direction		Y-direction	
	f /Hz	f/f_0	f /Hz	f/f_0	f /Hz	f/f_0
Initial	7.94	1.000	13.70	1.000	18.87	1.000
after 0.0875g	7.87	0.991	13.51	0.986	18.52	0.981
after 0.250g	6.54	0.824	12.82	0.936	17.54	0.930
after 0.550g	3.03	0.382	11.24	0.820	16.67	0.883
after 0.775g			9.90	0.723	15.39	0.816
after 1.000g			8.00	0.584	13.33	0.706
after 1.275g			5.99	0.437	11.11	0.589
after 1.550g			3.50	0.255	9.52	0.505

3.3 Acceleration response

The acceleration amplification factor (AAF), which is related to the dynamic characteristics of the structures and the spectral characteristics of the seismic ground motions, is an important parameter for the evaluation of the structural seismic response. In this section, the AAF is defined as the ratio of the recorded peak accelerations at the different locations to the maximum input acceleration. The evolutions of AAF along the height of the CS specimen and SS specimen subjected to different ground motions are shown in Fig. 9.

As shown in Fig. 9, the largest AAF was observed on the top of the test structures when they subjected to different ground motions of same intensity, indicating that there is an impact on the acceleration on the top of the structure. The AAF of the test structure varies depending on the ground motions, demonstrating that the spectral characteristics of the ground motion influence the structural response. Moreover, the AAF at the roof of the SS specimen is much greater than that of the CS specimen, the reason is that the stiffness of the strengthened structure is improved, the seismic load applied to the structure also increases, resulting in the increase of acceleration. For the SS specimen, the acceleration along X-direction is lower than the acceleration along the Y-direction, demonstrating that the stiffness in X-direction is smaller than the stiffness in Y-direction.

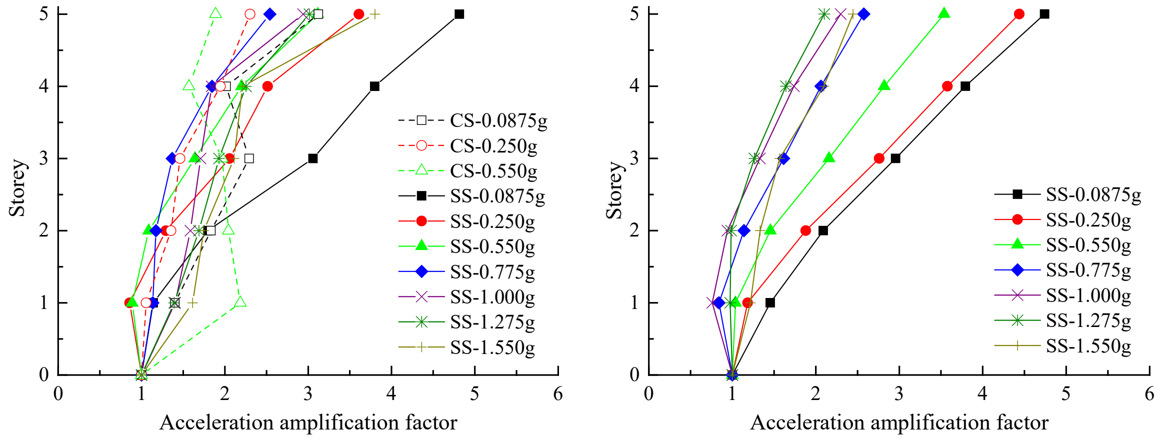

(a) El Centro; X-direction (b) El Centro; Y-direction

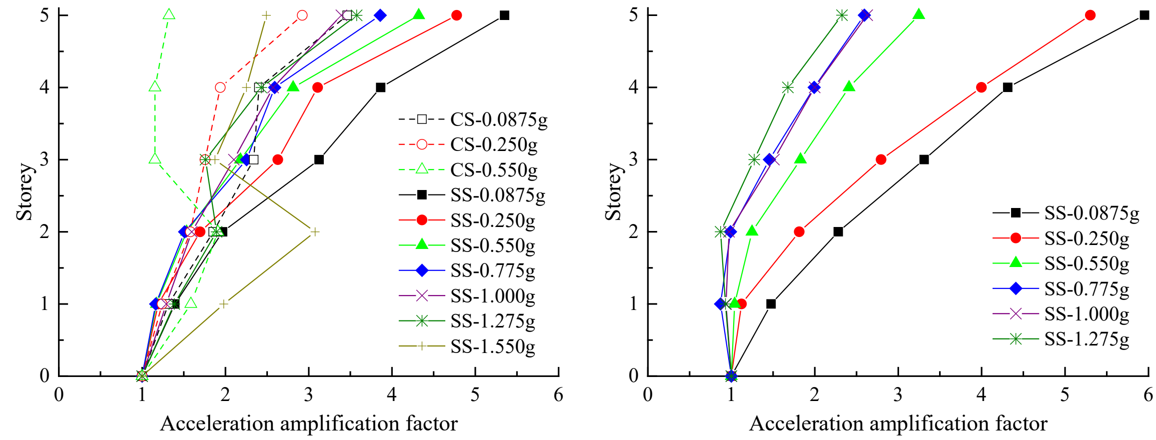

(c) Taft; X-direction (d) Taft; Y-direction

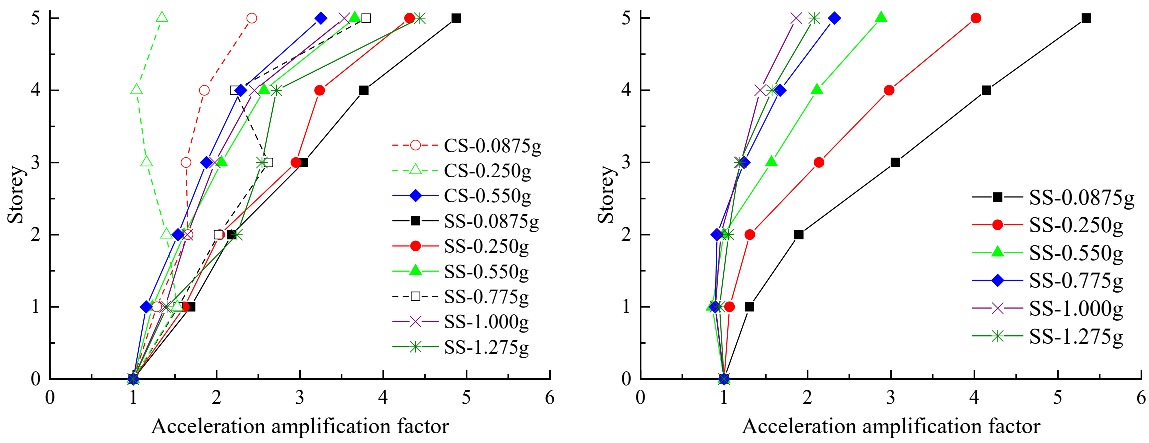

(e) SHW2; X-direction (f) SHW2; Y-direction

Fig. 9. Acceleration amplification factor of CS and SS specimens.

As the earthquake intensity increases, cracks continue to form, structural damage aggravates, and structural stiffness deteriorates, thus resulting in an overall negative trend of AAF, as shown in Fig. 10. However, in a specific range of the structure period (e.g. PGA larger than 0.775g for X-direction of SS specimen), AAF may increase with the increase of the structure period, as show in Fig. 10. The reason is that in a certain period, the S_a may first decrease and then increase with the increase of the period (see Fig. 6d). During PGA = 0.550g test stages, the masonry walls at the bottom of the CS specimen were severely damaged. The cracks had a dampening effect causing the AAF of each storey to exhibit a clear nonlinear distribution. Same behaviour was observed in the SS specimen during PGA = 0.550g test stages.

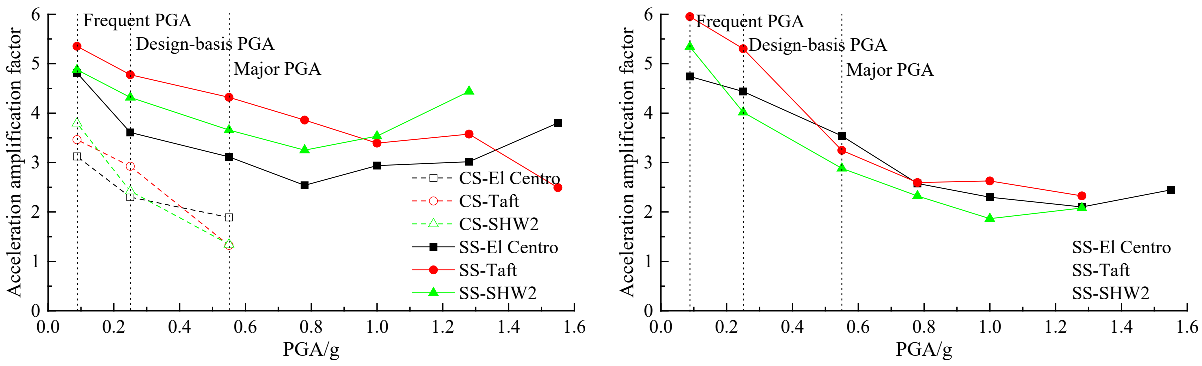

(a) X-direction (b) Y-direction

Fig. 10. Variation of roof acceleration amplification factor.

3.4 Storey drift response

Maximum storey drifts of each storey under the different seismic motions and intensity levels for the CS and SS specimen are shown in Fig. 11, respectively. The storey drifts of the CS and SS specimens increased by increasing the seismic intensity. During PGA = 0.550g test stages, the CS specimen was seriously damaged, the storey drifts were increased sharply, and the damage was most pronounced in the 2nd storey. During PGA = 1.550g test stages, the SS specimen was seriously damaged, and a sudden change of storey drift occurred in the 3rd storey.

Storey drifts in the X-direction of SS specimen were significantly reduced compared to those of OS specimen because of the higher stiffness of the former. During PGA = 0.550g test stages, the storey drifts in the X-direction of the CS and SS specimens are 1/142 and 1/605, respectively. The storey drift exhibited by the SS specimen was reduced by 76.6%. During the whole loading process, the storey drift along the X-direction of CS specimen reach its maximum value of 1/142 when PGA = 0.550g, while the storey drift along the X-direction of SS specimen reach its maximum value of 1/57 when PGA = 1.550g. The maximum storey drift of the CS specimen is 2.5 times higher that of the formers SS structure, indicating that the strengthening method effectively improves the storey deformation capacity of masonry structures.

According to Jiang et al.[32], five damage limit states, namely *Intact*, *Negligible*, *Minor*, *Moderate*, and *Severe*, have been proposed to describe the damage degrees of unreinforced masonry structures, where the corresponding drifts limits are 1/2500, 1/1330, 1/800, 1/500, and 1/330, respectively. The maximum storey drifts and damage states of the CS specimen under different seismic intensity are shown in Table 4. The result show that the damage state of CS specimen is *Intact*, *Moderate*, and *Collapse* after PGA = 0.0875g, 0.250g, and 0.55g test stages, respectively. The CS specimen was seriously damaged and the masonry wall of the 2nd storey collapsed during the shaking table tests of PGA = 0.550g.

The shear walls of SS specimen are UHDCC-masonry composite walls, and the drift limits of each damage limit states of the composite structures may fall between that of unreinforced masonry structures and that of reinforced concrete shear wall structures. Therefore, four damage limit states, namely *Negligible*, *Minor*, *Moderate*, and *Severe*, have been proposed to describe the damage degrees of strengthened masonry structures, where the corresponding drifts limits are 1/1000, 1/500, 1/250, and 1/120, respectively. The maximum storey drifts and damage states of the SS specimen under different seismic intensity are shown in Table 4. The results show that the SS specimen can meet the requirements of the specification [30], and the strengthened masonry structure exhibits sufficient seismic performance and ductility. The storey drifts in Y-direction of SS specimen are less than that in X-direction, indicating that the damage state in Y-direction of SS specimen is lighter than that in X-direction.

To investigate the influence of the strengthened method on structural torsion, the torsion angle of the structure, namely the displacement difference of *Dx*7 and *Dx*6 divided by their spacing, is taken for comparison before and after strengthening. After PGA = 0.550g test stages, the maximum torsion angles in the X-direction of CS and SS specimens reached 1/974 and 1/1903, respectively. The torsion angle exhibited by the SS specimen was reduced by 48.8%, indicating that the strengthened method can improve the integrity of masonry structures and significantly reduce the structural torsion.

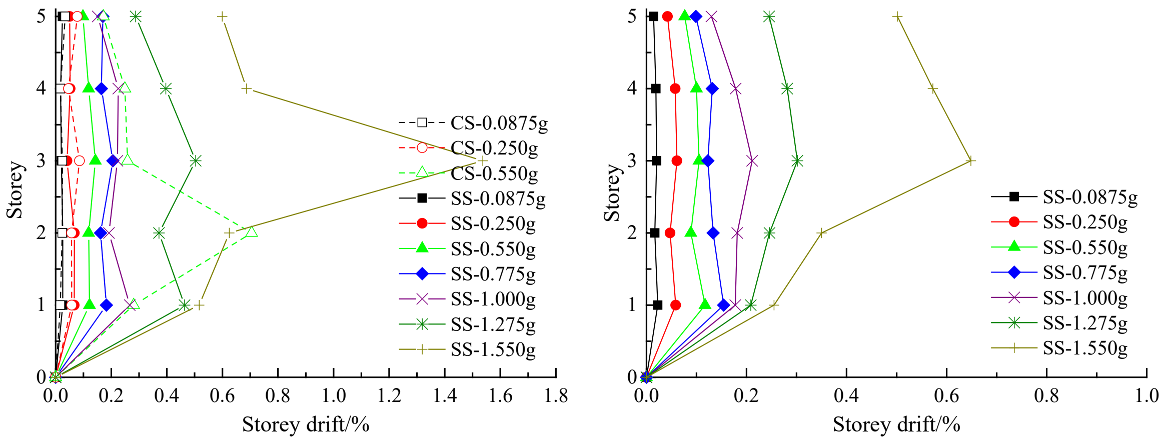

(a) El Centro; X-direction (b) El Centro; Y-direction

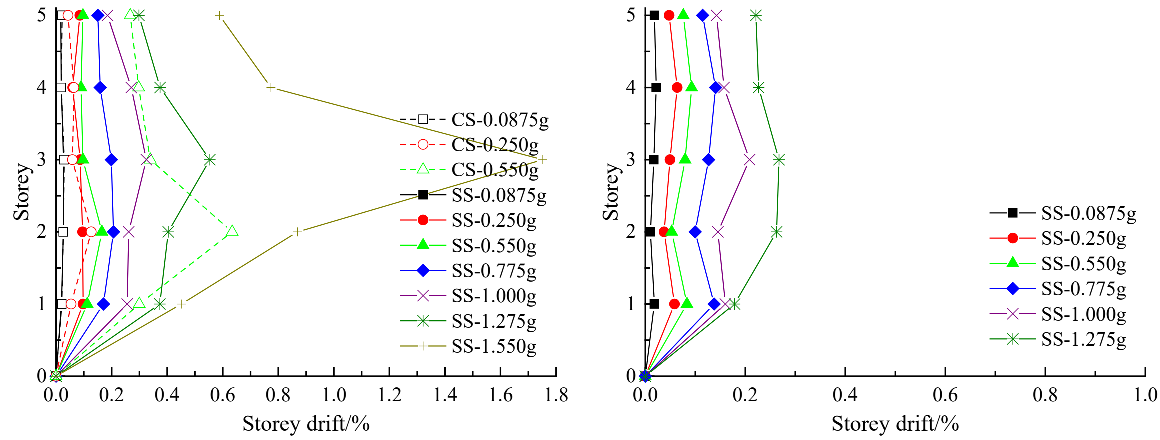

(c) Taft; X-direction (d) Taft; Y-direction

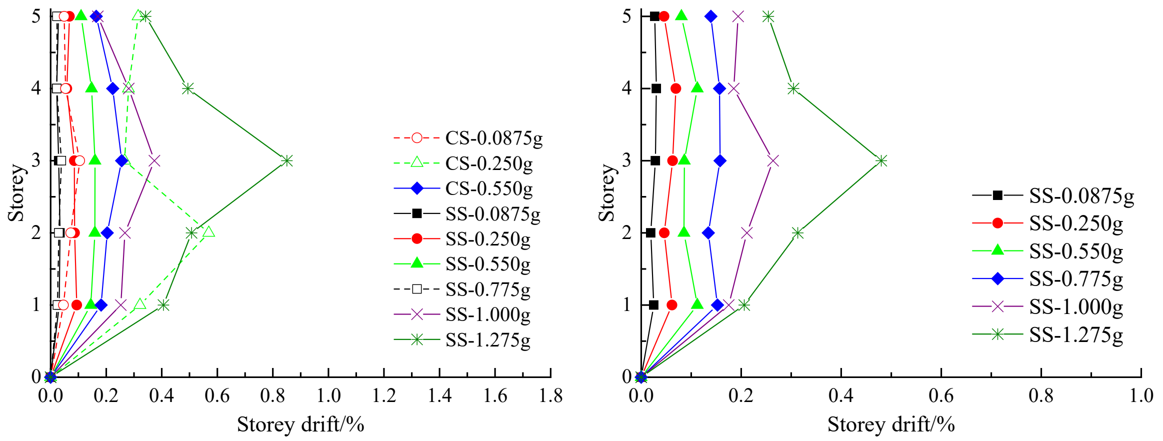

(e) Shanghai; X-direction (f) Shanghai; Y-direction

Fig. 11. Maximum storey drift of CS and SS specimens.

Table 4 The maximum storey drifts and damage states of the specimens

PGA/g	CS specimen		SS specimen	
	Maximum storey drift	Damage state	Maximum storey drift	Damage state
0.0875	1/2592	*Intact*	1/2968	*Negligible*
0.250	1/789	*Moderate*	1/1027	*Negligible*
0.550	1/142	*Collapse*	1/605	*Minor*
0.775			1/390	*Moderate*
1.000			1/267	*Moderate*
1.275			1/137	*Severe*
1.550			1/57	*Collapse*

3.5 Backbone curves

The base shear and the roof drift of the CS and SS specimens under the different seismic intensities are calculated. The base shear normalized by the specimen weight is plotted against the roof drift in Fig. 12.

The backbone curves of CS specimen in X-direction of the structure exhibit a bilinear relationship. The base shear reached during PGA = 0.250g test stages is basically similar to that during PGA = 0.550g test stages. This indicates that the CS specimen entered the elastic-plastic stage and structural stiffness degraded to a certain extent at PGA = 0.250g. The test specimen exhibited an obvious elastic-plastic deformation and severe stiffness degradation at PGA = 0.550g.

For shakings of PGA = 0.550g, the backbone curve of SS specimen in X-direction is approximately linear, indicating that SS specimen behaves elastically. For shakings of PGA = 1.000g, SS specimen in X-direction has entered in the plastic range and stiffness started to deteriorate. For shakings of PGA = 1.550g, the base shear of SS specimen is almost identical to that of PGA = 1.275g, indicating that the structure has suffered serious damage under the El Centro ground motion (PGA =1.550g).Before imposing the ground motions of PGA = 0.775g, the backbone curves of SS specimen in Y-direction are approximately linear. For shakings of PGA = 0.775g, SS specimen in Y-direction entered the plastic deformation stage. For shakings of PGA =1.550g, the base shear of SS specimen still increases due to less openings in Y-direction, indicating that the SS specimen along Y-direction can resist ground motions of a PGA = 1.550g.

The maximum base shear of CS specimen in X-direction is 35.2 kN, and that of SS specimen in X-direction is 167.6 kN. The maximum roof drift of CS specimen in the X-direction is 0.22%, and that of SS specimen in the X-direction is 0.75%. The lateral capacity and the maximum roof drift of the SS specimen was found to be 4.8 and 3.4 times that of the CS specimen.

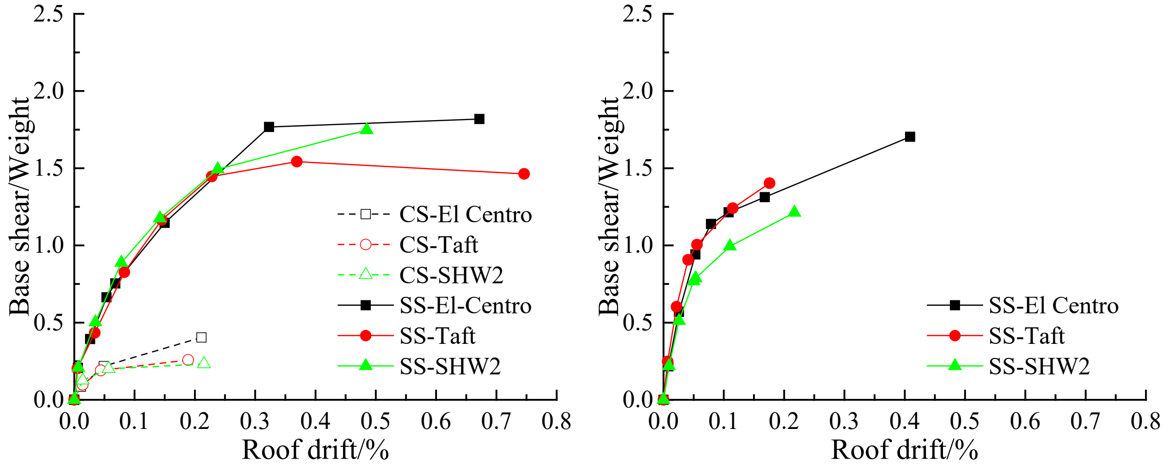

(a) X-direction (b) Y-direction

Fig. 12. Relationship curves in terms of the base shear vs. roof drift.

4. Conclusions

This study introduced ultra-high ductile cementitious composites (UHDCC) for strengthening existing multi-storey unreinforced masonry structures against earthquakes. The seismic performance of masonry structure strengthened by UHDCC layers were investigated through three-dimensional shaking table tests. The main conclusions are summarized as follows:

1. After the multi-storey unreinforced masonry structure was strengthened by UHDCC layers, the damage of the strengthened test structure (SS) subjected to ground motions was significantly reduced. The conventional test structure (CS) was seriously damaged after PGA = 0.550g test stages, and exhibited obvious brittle failure. The SS specimen suffered only minor damages after PGA = 0.550g test stages, and its failure mode can be characterized as ductile failure.
2. Relative sliding between masonry walls and UHDCC layers was not observed in the SS

specimen, even when the structure was severely damaged during PGA = 1.550g test stages, indicating that masonry walls and UHDCC layers were efficiently worked together.

3. The strengthening method can improve the stiffness of the masonry structure. The initial natural period of the SS specimen was found 0.58 times that of the CS specimen. After PGA = 0.550g test stages, the f/f_0 ratio of the CS specimen in X-direction decreased to 0.382 from 1.0, while the corresponding ratios for the SS specimen in X-direction decreased only to 0.818, demonstrating that the strengthening method can reduce the degradation of structural stiffness.
4. Maximum storey drifts in the SS specimen were significantly reduced compared to those of CS specimen. After PGA = 0.550g test stages, the maximum storey drift of SS specimen was reduced by 76.6%. The maximum roof drift of SS specimen was found to be 3.4 times that of CS specimen. The strengthening method can significantly improve the deformation capacity of masonry structures indicating a better plastic engagement of the whole structure.
5. The proposed strengthening method improved the base shear of the unreinforced masonry structure. The lateral strength of the CS specimen reached its peak value at a PGA = 0.250g, while the corresponding capacity of SS specimen reached its peak value at a PGA = 1.275g. The lateral capacity of SS specimen was found to be 4.8 times that of the CS specimen.

Since the proposed strengthening method is the combined strengthening method of ECC and UHDCC, it can be qualitatively concluded that the UHDCC strengthening method can improve the seismic performance of masonry structures, and further research is required to quantitatively analyze the effect of UHDCC on the seismic performance of masonry structures. Moreover, the strengthening object in this manuscript is a damaged masonry structure, and the reinforcement effect of strengthening method for undamaged masonry structures needs to be furtherly investigated.

CRediT authorship contribution statement

Xi Chen: Investigation, Methodology, Data curation, Writing - original draft.

Yongqun Zhang: Investigation, Writing – original draft, Funding acquisition.

Zhuolin Wang: Conceptualization, Supervision, Writing - review & editing, Project administration.

Jiangtao Yu: Conceptualization, Resources.

Konstantinos Skalomenos: Supervision, Writing - review & editing.

Qingfeng Xu: Investigation, Validation.

Declaration of Competing Interest

The authors declare that they have no known competing financial interests or personal relationships that could have appeared to influence the work reported in this manuscript.

Acknowledgements

The authors would like to acknowledge the financial support provided by Natural Science Foundation of Shanghai (Grant No. 21ZR1455000) and Shanghai Rising-Star Program (Grant No. 20QB1404700).

References

[1] Karababa F S, Pomonis A. Damage data analysis and vulnerability estimation following the August 14, 2003 Lefkada Island, Greece, Earthquake. Bull Earthq Eng 2011; 9(4): 1015-46.

[2] Paultre P, Calais E, Proulx J, Prépetit C, Ambroise S. Damage to Engineered Structures during the 12 January 2010, Haiti (Leogane) Earthquake. Can J Civil Eng 2013; 40(8): 777-90.

[3] Wang Z. A preliminary report on the Great Wenchuan Earthquake. Earthq Eng Eng Vib 2008; 7(2): 225-34.

[4] Sun B T, Yan P L. Damage characteristics and seismic capacity of buildings during Nepal Ms 8.1 earthquake. Earthq Eng Eng Vib 2015; 14(3): 571-78.

[5] Ghiassi B, Soltani M, Tasnimi A A. Seismic Evaluation of Masonry Structures Strengthened with Reinforced Concrete Layers. J Struc Eng 2012; 138(6): 729-743.

[6] Kadam S, Singh Y, Li B. Strengthening of unreinforced masonry using welded wire mesh and micro-concrete-behaviour under in-plane action. Constr Build Mater 2014; 54: 247-57.

[7] Carrillo J, Pincheira J A, Flores L E. Quasi-static cyclic tests of confined masonry walls retrofitted with mortar overlays reinforced with either welded-wire mesh or steel fibers. J Build Eng 2020; 27: 100975.

[8] Li W, Wang T, Chen X, Zhong X, Pan P. Pseudo-dynamic tests on masonry residential buildings seismically retrofitted by precast steel reinforced concrete walls. Earthq Eng Eng Vib 2017; 16(3): 587-97.

[9] Zhang Y, Lin X, Wang T, Skalomenos K. Seismic behavior of masonry walls strengthened by precast reinforced concrete panels with different connection details. Eng Struct 2021, 242: 112597.

[10] Santa-Maria H, Alcaino P. Repair of in-plane shear damaged masonry walls with external FRP. Constr Build Mater 2011; 25: 1172-80.

[11] Rahman A, Ueda T. In-plane shear performance of masonry walls after strengthening by two different FRPs. J Compos Construct 2016; 20(5): 1-14.

[12] Li V C, Leung C K Y. Steady-state and multiple cracking of short random fiber composites. ASCE J Eng Mech 1992; 188(11): 2246-64.

[13] Li V C, Wang S X, Wu C. Tensile strain-hardening behavior or polyvinyl alcohol engineered cementitious composite (PVA-ECC). ACI Mater J 2001; 98(6): 483-92.

[14] Li V C. On engineered cementitious composites (ECC): a review of the material and its applications. J Adv Concr Technol 2003; 1(3): 215-30.

[15] Lin Y W, Wotherspoon L, Scott A, Ingham J M. In-plane strengthening of clay brick unreinforced masonry wallettes using ECC shotcrete. Eng Struct 2014; 66: 57-65.

[16] Soleimani-Dashtaki S, Ventura C E, Banthia N. Seismic strengthening of unreinforced masonry walls using

sprayable ecofriendly ductile cementitious composite (EDCC). Procedia Eng 2017; 210: 154-64.

[17] Deng M K, Yang S. Cyclic testing of unreinforced masonry walls retrofitted with engineered cementitious composites. Constr Build Mater 2018; 177: 395-408.

[18] Maalej M, Lin V W J, Nguyen M P, Quek S T. Engineered cementitious composites for effective strengthening of unreinforced masonry walls. Eng Struct 2010; 32(8): 2432-9.

[19] Pourfalah S, Cotsovos DM, Suryanto B. Modelling the out-of-plane behaviour of masonry walls retrofitted with engineered cementitious composites. Comput Struct 2018; 201:58-79.

[20] Deng, M. K., W. Zhang, and N. Li. In-plane cyclic loading tests of concrete hollow block masonry walls retrofitted with high ductile fiber reinforced concrete. Constr Build Mater 2020; 238: 117758.

[21] Deng M K, Z F Dong, Wang X S, Zhang Y X, Zhou T G. Shaking table tests of a half-scale 2-storey URM building retrofitted with a high ductility fibre reinforced concrete overlay system. Eng Struct 2019; 197: 109424.

[22] Wang Y C, Wei L Z, Yu J T, Yu K Q. Mechanical properties of high ductile magnesium oxychloride cement-based composites after water soaking. Cem Concr Compos 2019; 97: 248-58.

[23] Yu J T, Dong F Y, Ye J H. Experimental study on the size effect of ultra-high ductile cementitious composites. Constr Build Mater 2020; 240: 117963.

[24] Yu J T, Jiang F M, Yu K Q, Dong F Y, Duan X Z. Deformability enhancement of fiber-reinforced cementitious composite by incorporating recycled powder. J Reinf Plast Compos 2020; 39(3-4): 119-31.

[25] Yu J T, Ye J H, Zhao B, Xu S L, Wang B, Yu K Q. Dynamic response of concrete frames including plain ductile cementitious composites. J Struct Eng 2019; 145 (6): 04019042.

[26] Dong F Y, Yu J T, Zhan K L, Li Z H. Seismic fragility analysis on ultra-high ductile cementitious composites frame without steel reinforcement. Adv Struct Eng 2020; 23 (11): 2373-87.

[27] GB/T 2542-2012. Test methods for wall bricks. Beijing, China: China standard Press; 2012. [in Chinese]

[28] JGJ/T 70–2009. Standard for test method of performance on building mortar. Beijing, China: China Architecture & Building Press; 2009. [in Chinese]

[29] GB/T 50129–2011. Standard for test method of basic mechanics properties of masonry. Beijing, China: China Architecture & Building Press; 2011. [in Chinese]

[30] GB50011-2010. Code for seismic design of buildings. Beijing, China: China Architecture & Building Press;

2010. [in Chinese]

[31] Zhang Y, Wang Z, Jiang L, Skalomenos K, Zhang D. Seismic analysis method of unreinforced masonry structures subjected to mainshock-aftershock sequences. Bull Earthquake Eng (2022); https://doi.org/10.1007/s10518-022-01334-x.

[32] Jiang L, Wang Z, Zhang F. Damage degree and inter-story drift angle limit of multi-story masonry structures. Journal of Building structure 2018; 39: 263-270. [in Chinese]